Journal of Systems Engineering and Electronics
Vol. 28, No. 6, December 2017, pp.1221 – 1235

Enhancing of nominal characteristic trajectory following control for motion systems

Fitri Yakub[1,4,*], Shamsul Sarip[2], Andika Aji Wijaya[3], and Yasuchika Mori[4]

1. Malaysia-Japan International Institute of Technology, University of Technology Malaysia, Kuala Lumpur 54100, Malaysia;
2. Razak School of Engineering and Advanced Technology, University of Technology Malaysia, Kuala Lumpur, 54100, Malaysia;
3. Department of Industrial Engineering, University of Business and Technology, Jeddah 21361, Saudi Arabia;
4. Graduate School of System Design, Tokyo Metropolitan University, Tokyo 191-0065, Japan

Abstract: The goal of this paper is to enhance a practical nominal characteristic trajectory following (NCTF) controller that is specifically designed for two-mass point-to-point positioning systems. A nominal characteristics trajectory contained in the NCTF controller acts as movement/motion reference and a compensator is utilized to force the object to detect and follow the reference/desired trajectory. The object must follow and track closely and should be as fast as possible. The NCTF controller is designed with two different intelligent based compensator approaches which are fuzzy logic and extended minimal resource allocation network. The proposed controller which is NCTF are compared with the conventional proportional integral compensator. Then the results of simulation are discussed for the positioning performances. The inertia variations due to the effect of the design parameters are also assessed to see the robustness of controllers. The results show that the NCTF control method designed from an intelligent based compensator has a better positioning performance in terms of percentage of overshoot, settling time, and steady state error than the classical based compensator.

Keywords: two-mass rotary system, intelligent approach, classical method, mechanical vibration, nominal characteristic trajectory following.

DOI: 10.21629/JSEE.2017.06.20

1. Introduction

The precision positioning systems along with electromechanical drives, sensors and a controller are broadly employed in many industrial machines applications, such as semiconductor systems, computer numerical robot systems and control machining. There are particular devices of mechanical tools in multi-mass systems that particularly contain low natural frequency of vibrations which is also known as resonant frequency. Due to this characteristic, the limited amplitude but small elastic deflection of gears and rotating shaft might get enlarged. The examples of mechanical elements in multi-mass systems are long shafts with less stiffness, large roll inertia, machine tools spindles and gear boxes. Besides, the oscillation has an effect on the load. As a result, there might be some problem occurring on the systems. Thus, the systems will become unstable, poor in positioning accuracy and possibly damaged [1].

Moreover, the point-to-point (PTP) control system is often applied to mechanical elements having friction and exhibiting spring-like behavior [2] in a narrow working band. These nonlinearities, i.e. friction and saturation which usually becomes the root cause for actuators in all devices having comparative motion occur in all mechanical systems. As a result, the motion in the mechanism will be interrupted and it will lead to steady state error and make the system to be unstable [3]. There are many approaches that have been demonstrated costly in order to improve the mechanism elements for precise and great positioning achievement [4].

Therefore, numerous controller architectures acquired are developed and suggested in PTP positioning systems including proportional integral derivative (PID) [5], robust PID controllers [6], predictive controllers [7], time optimal controllers [8], sliding mode controllers [9], and disturbance observer controllers [10]. Since transient performance of the control systems [11] is very important in many control applications, various methods are proposed in the literature to address the transient performance of the control systems, e.g. robust control with adaptation mechanism [12], low and high gain controls [13], fixed-order control [14], to name just a few. Most of the results focus on the solvability of the investigated issues while the transient response of the closed-loop system is not well addressed.

To enhance the transient response of the closed-loop

Manuscript received August 07, 2015.
*Corresponding author.

system for the tracking control problem, composite nonlinear feedback (CNF) control was first proposed in [15] for a class of second-order linear system with input saturation. The applications of the CNF control method are also described in the literature, such as, servo position system [16] and direct current (DC) motor system [17].

Nevertheless, the conventional controllers have some difficulties to keep the response without getting an overshoot because of their limitations on the robustness of the performance and the higher positioning. On the other hand, to determine the exact model plant of the advanced controllers, it needs a longest period of time to identify its parameters. Rapid reaction and less overshoot are attractive in most of the tracking control difficulties. Nevertheless, it is well known that rapid reaction results in a huge overshoot. Hence, most of the control design structures have to compromise among these two transient response indices.

From the previous study in 2001, a nominal characteristic trajectory following (NCTF) control was designed and implemented succesfully in order to encounter the problem occurring in the previous study. A single-mass rotary positioning system [18 – 20] was successfully implemented. Besides, the NCTF control can be employed in many practical applications problems and the comprehensive knowledge of the theoretical circumstanses as it is a practical controller. The advantages of the NCTF control design method are flexible, straightforward, and simple in implementation as well as easy to understand. Since it is a simple system design, the parameter and the mathematical model of the system are not required as this controller only depends on the simple open-loop response of the system [21].

An NCTF control has been implemented in real mechanisms and it has been reported to have a better positioning performance than the classical PI/PID controller for a single-axis motion system [22 – 26] and for a two-mass system [27], and to be more robust under parameter variations [28,29]; and it has been successfully implemented with mechanisms having friction [30,31]. The best comparative study on NCTF control strategies for motion systems can be found in [32,33], where single- and two-mass positioning systems used with linear and rotary systems are explained. To the best of the authors' knowledge, there has been no comparative study of NCTF control for multi-mass system for PTP positioning systems, which is discussed in this paper.

The NCTF control concept designed in [34] and [35,36] are extended for distinctive compensator design approached in a rotary motion system emphasizing on two-mass to achieve precise and accurate control performance. Then, the robustness and the positioning of the system are compared by using three different types of compensators designs which are fuzzy logic (FL) control, proportional integral (PI) control, and extended minimal resource allocation network (EMRAN) control.

The main goal of this paper is to broaden the application of the NCTF controller as well as to compare the effectiveness of the positioning performance of the NCTF control by using different types of compensator design. Next, the designation of the NCTF controller is improvised on its design of nominal characteristic trajectory (NCT) in order to see whether multi-mass positioning systems can adapt with the NCTF controller or not. This study also explains a vibration dilemma raised by the mechanical resonance of the plants and proposes its simple solution with a practical and systematic design method. The efficiency of the proposed controller and its design approach are demonstrated through simulation results.

This paper will be structured as follows. The system model and the basic concept of NCTF control are described in Section 2. Meanwhile in Section 3, the PI, FL, and EMRAN compensator designs are studied and well explained. Section 4 gives the results of the simulations of movement control accomplishment of the proposed NCTF control system. The results are analyzed and distinguished based on positioning motion and robustness performances. Last but not least, Section 5 describes the conclusion and the possible future work.

2. Scheme and control theory

2.1 System scheme

The model of the system is defined in [1] to derive all the unit measurements, and the international system of units (SI) is used for entire physical quantities and valid for entire notations. In this paper, the simulation is done by using the exact parameters from the real object [1].

The exact block diagram of the plant for the simulation purposes is also described in [1]. In this model, several disturbances are taken into account, such as friction and saturation. Therefore, whether the controllers can adapt for high precision positioning systems or not can be seen by enhancing the NCTF controller design. Hence, a multi-mass motion system could satisfy the high precision positioning systems since the controller is more likely to be reliable, accurate and effective.

The transfer function form of the simplified model of the two-mass positioning system is written in the fourth-order system:

$$G_o(s) = \frac{\theta_l(s)}{U(s)} = K\frac{\alpha}{s(s+\alpha)}\frac{\omega_f^2}{s^2+2\zeta_f\omega_f s+\omega_f^2} \quad (1)$$

where K, ζ_f, α, and ω_f indicate the variables of the simplified plant which needs to be resolved. Fig. 1 shows the open-loop responses for single-mass and two-mass in order to clarify that two-mass contains the vibration effect.

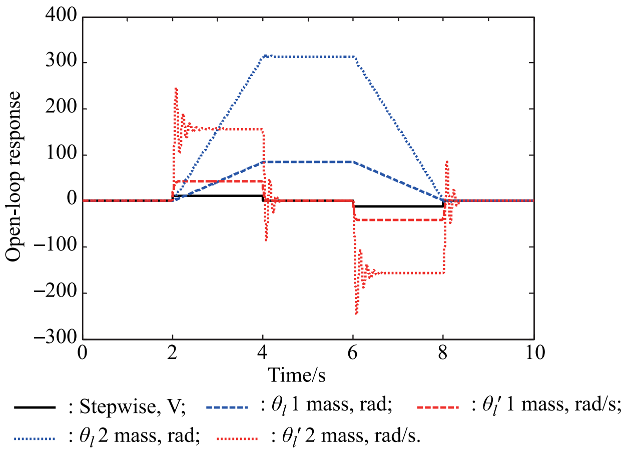

Fig. 1 Open-loop response of single/two-mass systems

2.2 NCTF control theory

The basic structure of the NCTF control mechanism is illustrated in Fig. 2. There are two main subsystems in this plant, which are a nominal characteristic trajectory and a compensator. The NCT is a chosen path that is built from uncomplicated and fast open-loop response. Other than that, it is not a necessarily required mathematical model while the compensator is designed based on the parameters acquired from the NCT. The significant target of the compensator for NCTF approach configuration is to produce the desired motion in order to track the target trajectory so that the object movement will stop at the desired point.

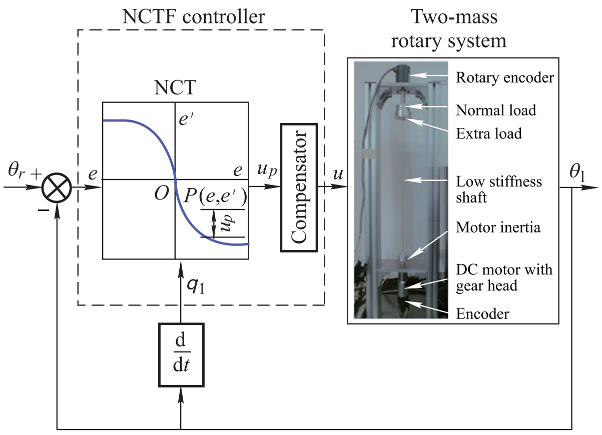

Fig. 2 General block diagram of NCTF control system

The scenario mentioned above is perhaps examined from the phase plane (e, e') illustrated in Fig. 2. The signal u_p is adopted as a signal input for the compensator so that the actual object motion will follow exactly the targeted NCT without failure. Therefore the value of u_p can be zero. This criteria will reflect the aim of the compensator in NCTF where the actual object motion is controlled by the NCTF method so that the signal u_p is equal to zero. The fundamental concept of the NCT controller can be found in [21] and [28].

A DC motor acts as an actuator to the system. The function of the actuator is to drive the plant or object to reach the desired NCT. It is also known that, the actuator/motor specification characteristic when it ends from its maximum velocity or ultimate input, will influence and deteriorate the final accuracy and efficiency of the PTP positioning performance. Hence, this actuator behavior is needed to design the NCTF controller. In order to achieve the required actuator characteristics, performing an easy open-loop experiment or real-time response is a practical and simple method.

3. Controller scheme

3.1 NCT structure

The stepwise input is used for an open loop performance to control the actuator in order to create the NCT. Subsequently, the real object vibrates because the effect forms its mechanical resonance. Hence, the output responses for the feedback on the real object movement are determined in terms of load velocity and displacement illustrated in Fig. 3. All the output performances are built from the original rotary systems along with a low stiffness shaft. As opposed to the single-mass system, there is no vibration effect, and thus the NCT can be easily determined as shown in Fig. 4.

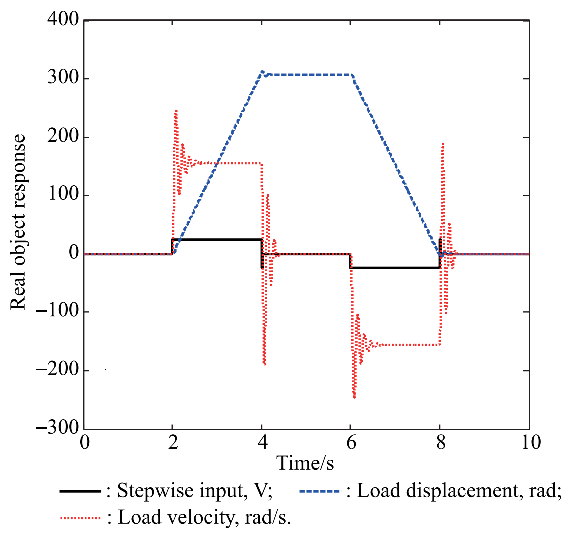

Fig. 3 Signal input and real object response

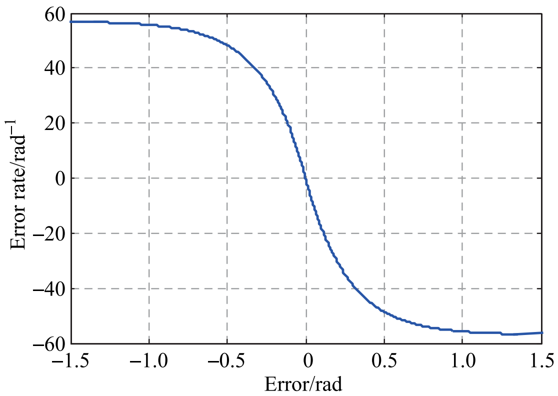

Fig. 4 NCT of single-mass system

However, the effect of vibration in two mass systems must be eliminated in order to determine the trajectory of NCT. Besides, the product from the system of the object responses should be normalized. In this paper, a smooth moving average filter (MAV) is executed from [37]. To determine the NCT, the averaged outcome object performances of the plant are employed as shown in Fig. 5.

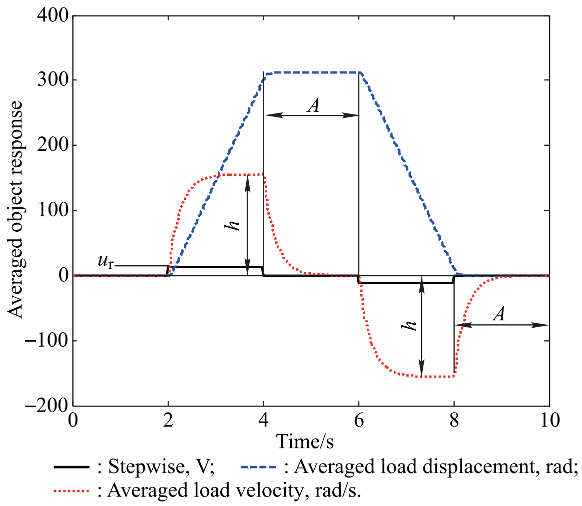

Fig. 5 Signal input and averaged object response

From Fig. 5, the MAV is applied in the system to get the averaged response due to its easiness. By estimating the number of points from the object performances, the MAV is obtained to get each point of the averaged operation. The following equation is stated as below:

$$\begin{cases} \theta_{l,av}(i) = \dfrac{1}{M}\displaystyle\sum_{j=-(M-1)/2}^{(M-1)/2} \theta_l(i+j) \\ \dot{\theta}_{l,av}(i) = \dfrac{1}{M}\displaystyle\sum_{j=-(M-1)/2}^{(M-1)/2} \dot{\theta}_l(i+j) \end{cases}. \tag{2}$$

In MAV concept, the filter parameter M is the number of points in the average. In order to get a good averaging result, the number of points M is set to be equal to the number of points in one cycle of the vibration as follows:

$$M = \frac{\omega_s}{\omega_{fd}} \tag{3}$$

where ω_s represents a sampling rate and ω_{fd} represents the vibrating frequency of the object responses in rad/s. In this MAV, index i is the point in the average signal, while index j is the running point. It is also known that MAV is a convolution using a very simple filter kernel.

In order to determine the NCT motion, there are two criteria to be considered, which are averaged responses of displacement and velocity. Meanwhile for the PTP motion approach, we would like to get faster desired output without an overshoot and the object motion must stop at a certain position without any error. Therefore, the deceleration process is shown by the curve A in Fig. 5 whereas Fig. 6 represents the NCT determination in which the maximum velocity h is applied in the system. To determine the height of the stepwise input, the maximum velocity and the deceleration process are considered. There are two valuable parameters in the NCT, which are the inclination of the NCT close to the origin m, and the maximum error rate h. These parameters observed are illustrated in Fig. 6 and used in order to design a compensator since both parameters are connected to the dynamic behaviors of the actual object.

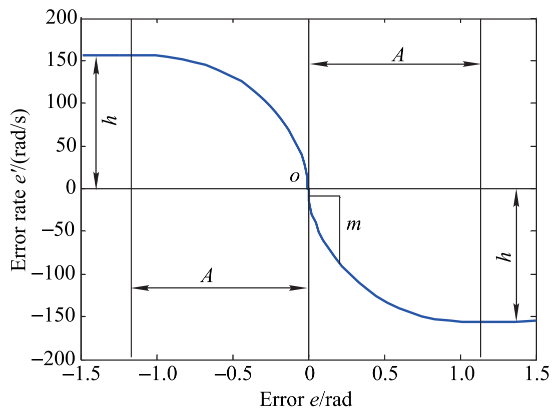

Fig. 6 NCT of the two-mass system

Since the actual output responses in the two-mass system have the vibration effect, thus NCT cannot be constructed from the actual responses due to high oscillation from the system. Therefore, we need to use MAV to average the actual output responses in order to construct the NCT. The NCT does not include the vibration effect since it depends on the averaged output responses that minimize the order of the system. Therefore, the following second order equation can be written as

$$\frac{\theta_{lav}(s)}{U(s)} = K\frac{\alpha}{s(s+\alpha)} \tag{4}$$

where α and K define the simplified averaged object variables. These parameters are linked to h and m in the data of NCT that are well elaborated in [21] for a single-mass motion system.

For the PTP motion system, the structure of the NCTF control system only works under the following two conditions. First a DC motor acts as an actuator of the object, and second, the reference input θ_r is constant since it controls the motion system, and its derivative $\theta_r = 0$, which produces the error, $e = \theta_r - \theta_l$, and the reaction of NCT which is given by the value of h is connected with hypothesis of the final value for the steady-state velocity due to the input actuator which can be given as $h = Ku_r$.

3.2 Vibration elimination

A shaft acts as coupling among the motor and the object mass can have very low stiffness functioning like a spring which may cause an oscillation or vibration at the resonance frequency, resulting in an unstable system in a two-mass rotary system. The averaged position response in (4) does not represent the real two-mass system as in (1). Hence the vibration effect on the system cannot be eliminated because the NCT parameters determination is not effective in the system in (1) without a filter. Hence a filter is used in the compensator structure design. The simple and effective method which is an anti-resonance notch filter (NF) [38] is used in order to compromise along the torsional resonance in the system in (1). The transfer function of the NF is given by the following equation:

$$G_{nf}(s) = \frac{K_{dc}(s^2 + 2\zeta_f\omega_f s + \omega_f^2)}{(s^2 + 2\zeta_o\omega_o s + \omega_o^2)}. \quad (5)$$

A notch filter consists of a pair of complex zeros and a pair of complex poles as illustrated in (5). The complex poles, which are characterized by ω_o and ζ_o are used to create an additional resonance, where if the magnitude of the real value of the poles is large enough, it will result in a well damped response. These complex poles are also used to increase the gain margin of the overall system. On the other hand, the purpose of the complex zeros defined by ω_f and ζ_f is to cancel the resonance poles of the system that eliminate the vibration caused by mechanical resonance.

In order to cancel out the resonant frequency of the system, the ratio between ζ_f and ζ_o is employed to determine how deep the notch of the NF is. The last parameter of NF is the gain K_{dc} used in the steady state condition when the transfer function of the NF becomes one. In this paper, perfect cancellation of the resonance poles by NF is not necessary since NF can adequately reduce the effect of the vibration as long as the zeros of NF are close enough to the original plant poles.

From the system parameters in [1], the poles and zeros are located on the s-plane, as shown in Fig. 7, which illustrates that the system is unstable without the controller from the system's root locus. Fig. 8 shows the effect of the implemented NF that makes the overall system become stable by the cancellation of the complex zeros marked by B to the poles marked by A caused by the mechanical resonance of the plant.

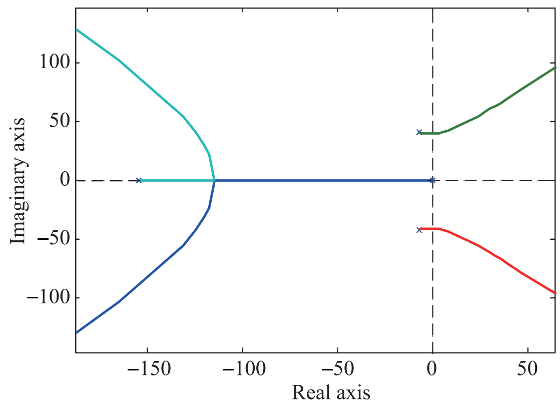

Fig. 7 Root locus of the system

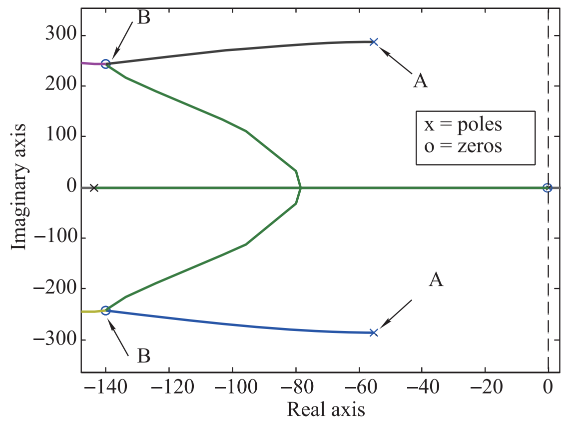

Fig. 8 Pole-zero cancellation of the notch filter

Another effect of the NF on the plant in order to eliminate the vibration and reduce the magnitude of oscillation can be seen through the time domain analysis as shown in Fig. 9. It should be highlighted here that complete cancellation of the system's resonance poles by the NF is not necessary, because as long as the zeros of the NF are nearest to or approaching the original poles of the system, the NF can sufficiently decrease the vibration/oscillation effect, and therefore improve the system response. In this work, we do not focus detail on the design of the NF because this can be found in [1]. Therefore, we will use the same design parameters for the NF for all the compensator structures throughout this paper.

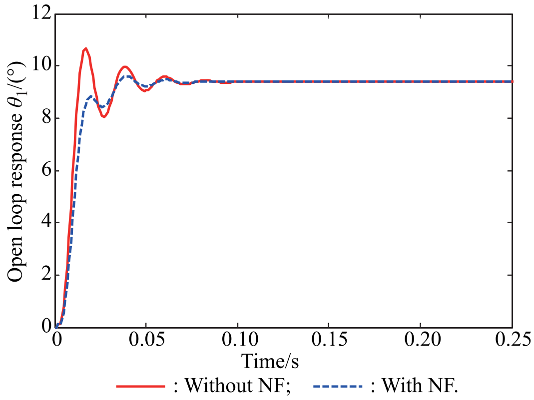

Fig. 9 Notch filter effect on the system in time domain

3.3 Compensator design

Since NCT in Fig. 6 has been designed based on averaged output responses as described in subsection 3.1, the simplified object model of (4) is expressed in the state-space equation:

$$\frac{\mathrm{d}}{\mathrm{d}t}\begin{bmatrix}\theta\\ \dot{\theta}\end{bmatrix} = \begin{bmatrix}0 & 1\\ 0 & -\alpha\end{bmatrix}\begin{bmatrix}\theta\\ \dot{\theta}\end{bmatrix} + \begin{bmatrix}0\\ \alpha K\end{bmatrix} u. \tag{6}$$

It is such an important aspect when the motion system characteristic is near to the reference position because the system stability and accuracy depend on their characteristics as explained in the NCTF control concept. In Fig. 6, the inclination of the NCT close to the origin is connected to the simplified object parameter α as

$$\frac{\mathrm{d}\dot{e}}{\mathrm{d}e} = m. \tag{7}$$

The NCT inclination close to the origin is constructed when the actuator/input to the object/target is zero ($u = 0$). Thus, (6) becomes

$$\frac{\mathrm{d}\dot{\theta}}{\mathrm{d}\theta} = -\alpha. \tag{8}$$

For the case of PTP positioning system, θ_r is constant and the positioning error is given by $e = \theta_r - \theta_l$, hence, (8) can be translated to

$$\frac{\mathrm{d}\dot{e}}{\mathrm{d}e} = -\alpha. \tag{9}$$

Therefore, from (7) and (9), we attain

$$\alpha = -m. \tag{10}$$

The value of the utmost error rate of the NCT is connected to the steady-state velocity of the object because of input actuator u_r. Through formulation of the final value theorem, the steady-state velocity is given as Ku_r. Then,

$$h = -Ku_r. \tag{11}$$

Thus, K can be conveyed as

$$K = \frac{h}{u_r}. \tag{12}$$

Since the object is performed based on real time open-loop experiment, the simplified object model includes the effect of friction. This friction feature induces the maximum error rate of the NCT and the inclination of the NCT near the origin.

3.3.1 PI compensator

The following PI controller is adopted in this work because it does not involve complex mechanism and is created from the object variables linked to h and m in the nominal trajectory that have been simplified, which is given by

$$G_{\mathrm{PI}}(s) = \left(\frac{K_p s + K_i}{s}\right). \tag{13}$$

From Fig. 2, the common NCTF configuration is designed toward a block diagram of the stable closed-loop control system though the trajectory is linear which happens when the object is close to the root that acquires inclination $\alpha = -m$ as illustrated in Fig. 10 and Fig. 11. The signal u_p indicates the error among the desired NCT with a real object motion as illustrated in Fig. 11. The consecutive equation in phrases of error and error rate can be written as

$$u_p = \dot{e} + \alpha e = \alpha e - \dot{\theta}_l. \tag{14}$$

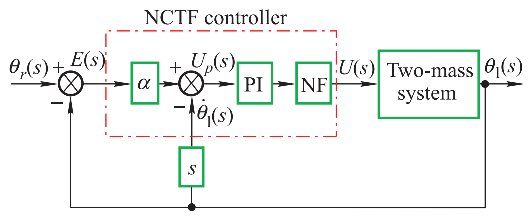

Fig. 10 Linearized NCTF control system at small error *e*

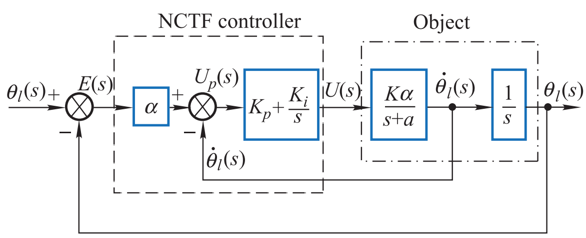

Fig. 11 Linearized of simplified NCTF control system at small error *e*

Based on the simplified object model in (4), with the PI compensator parameters K_p and K_i, the NCTF controller in Fig. 2 can be linearized in order to obtain the transfer function near the origin of the closed-loop system as

$$\frac{\theta_l(s)}{\theta_r(s)} = \frac{\alpha}{(s+\alpha)}\frac{\alpha K K_p s + \alpha K K_i}{(s^2 + \alpha K K_p s + \alpha K K_i)}. \tag{15}$$

By defining $\alpha K K_p = 2\zeta\omega_n$ and $\alpha K K_i = \omega_n^2$, (15) is rewritten in the following form:

$$\frac{\theta_l(s)}{\theta_r(s)} = \frac{\alpha}{(s+\alpha)} G(s) \tag{16}$$

where

$$G(s) = \frac{2\zeta\omega_n s + \omega_n^2}{s^2 + 2\zeta\omega_n s + \omega_n^2}. \tag{17}$$

In the case without any motion error, $G(s) = 1$, thus, (16) yields

$$\frac{\theta_l(s)}{\theta_r(s)} = \frac{\alpha}{(s+\alpha)}. \tag{18}$$

For motion systems, (18) can be revised in time domain as follows:

$$\dot{e} + \alpha e = 0. \tag{19}$$

From (14), the parameters gain of the PI controller can be written in the form of natural frequency ω_n together with damping ratio ζ as shown in the following equation (20). When the real object motion pursues the targeted NCT where the subsequent equation is used without having an error given by $G(s) = 1$, where the signal u_p will be zero.

$$K_p = \frac{2\zeta\omega_n}{\alpha K} = \frac{2\zeta\omega_n u_r}{mh} \tag{20}$$

$$K_i = \frac{\omega_n^2}{\alpha K} = \frac{\omega_n^2 u_r}{mh} \tag{21}$$

3.3.2 FL compensator

There are two inputs and one output given by the standard fuzzy compensator configuration as illustrated in Fig. 12 in which u_o stands for the output while the two inputs are denoted by the input signal u_p that reaches about the path, and the second fuzzy input signal represents the integration of u_p, that is u_i. The triangular-form fuzzifier of the fuzzy compensator known as the Mamdani method is used in this paper. This type of method consists of crisp parameters in pair of fuzzy input and fuzzy output. The entire variables inside the fuzzy compensator are adopted only primarily based on the NCT specifications because the approach of NCTF is straightforward.

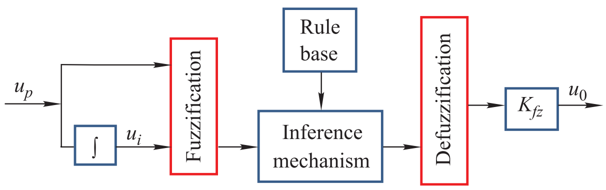

Fig. 12 Fuzzy compensator scheme

Membership function: Fig. 13 shows the membership function of the fuzzy compensator u_p, along with triangular configurations which are negative (N), zero (Z) and positive (P), acts as a membership function. The dimension of the input signal is indicated by $\pm h$ of the course where the signal u_p is indicated in (14) since the fuzzy signal u_p can be bounded by the length of the minimum and maximum h representing an output velocity of the plant. For the Z membership function indicated by the subsequent equation, e_r represents the error margin of the resolution encoder, while $\dot{e}_r$ denotes the error rate near to e_r.

$$\mu_{u_p} = \pm(\dot{e}_r + \alpha e_r). \tag{22}$$

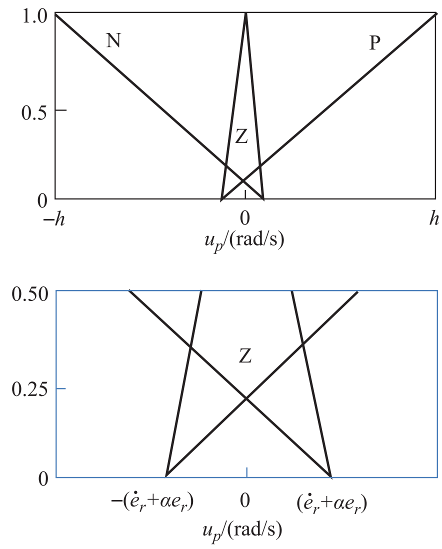

Fig. 13 Membership function of fuzzy input u_p

The range of fuzzy input $u_{i\,\max}$ (see Fig. 14) for the second input signal is imitative from the subsequent equation:

$$u_{i\,\max} = \int_0^{e_m} u_p \mathrm{d}e \cong \frac{1}{2} Ah. \tag{23}$$

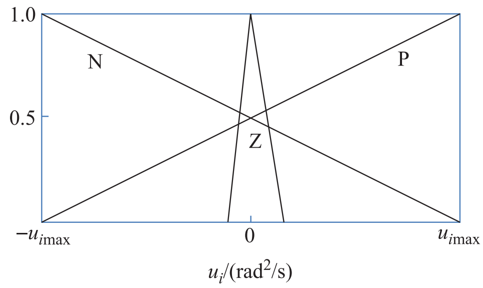

Fig. 14 Membership function of fuzzy input u_i

The variable values of A and h are obtained through the NCT as defined in Fig. 6. In the end, the fuzzy compensator output u_o as illustrated in Fig. 15 includes three fuzzy singleton forms N, Z, and P along the dimension of minimum and maximum of input u_r whereas the input rate about motor actuator $\pm u_r$ is represented in the real applications.

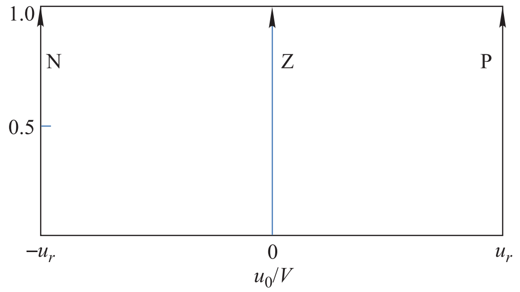

Fig. 15 Membership function of fuzzy output u_o

Fuzzy rule: The fuzzy compensator is used in order to produce and force the target motion to follow and track the trajectory reference as fast as possible. Therefore, the fuzzy compensator can contribute positive input to the system actuator provided that both inputs u_p and u_i are positive and vice versa.

To accomplish the following phase obligation, yet u_p is negative or positive and u_i is zero, the input of the plant actuator should be negative or positive. This is to ensure that the object motion strictly pursues the desired NCT. The target of the motion control is expected to stop at the origin of the phase plane in the final phase by setting the fuzzy n puts which are u_p and u_i to zero, the actuator supposed to be zero also when u_p is negative or positive and u_i is positive and negative accordingly. Table 1 outlines the fuzzy rules aiming for easy understanding.

Table 1 Fuzzy rules

Load object		u_p		
		N	Z	P
u_i	N	N	N	Z
	Z	N	Z	P
	P	Z	P	P

Fuzzy inference and defuzzification: Fuzzy interface is implemented for the fuzzy compensator scheme by using the Mamdani fuzzy model through the min-max method. Hence, the fuzzy control output u_o is calculated as

$$\mu_{u_0} = \min\lfloor \mu_{u_p} \max \mu_{u_i} \rfloor \tag{24}$$

where μ_{up} and μ_{ui} are the degree of membership functions of the fuzzy compensator inputs u_p and u_i accordingly, and μ_{uo} refers to the degree of the membership function of the fuzzy control output u_o. While in the defuzzification process, a fuzzy input value is converted back from the linguistic variable into the crisp fuzzy control output value given by the center of gravity equation:

$$u_o^* = \frac{\displaystyle\int_u \mu_{u_o}(u)u\mathrm{d}u}{\displaystyle\int_u \mu_{u_o}(u)\mathrm{d}u} \tag{25}$$

where u_o^* represents the defuzzified output, u_o refers to the output variable, and $\mu_{u_o}(u)$ represents the aggregated membership function.

Fuzzy gain K_{fz}: The fuzzy gain aims to grant the fuzzy inputs u_p and u_i with small values in order to fire the fuzzy rule. This fuzzy gain K_{fz} has correlation to NCT parameters while pursues

$$K_{fz} = \frac{h}{u_r}. \tag{26}$$

3.3.3 EMRAN compensator

A quick learning can be achieved with the minimum resource of distributing the network and it also may be assigned as an online or true time based learning algorithm. The radial based function network (RBFN) is used in this paper as an alternative way of a standard neural network because it has a problem of dimensionality. In order to train the network, the EMRAN algorithm is used. The number of neurons of the RBFN will gather to or diminish until the relevant result is achieved throughout the training. The parameters are improved using a strategy of "conqueror takes it all". It indicates that the most energized neurons on parameters of RBFN are improved or updated and the others will remain constant. With the only success neurons that will be improved, it can make the process minimize the total of the computational load time, and finally can lead to crucial decrease in the numbers of the parameters that are required to be improved online.

A fundamental scheme of the RBFN model together with the Gaussian function as modified to the current system is shown in Fig. 16. The number of hidden nodes a_N in the RBFN are appointed for the input, mapping u_p to the output control law u_n. The center position μ_j is for all j hidden neurons, σ_j is the width for Gaussian action values, and α_j is the relation weight which survives between the output layer and the jth hidden lager.

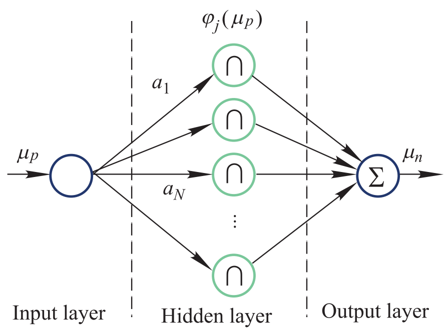

Fig. 16 Structure of radial basis function network

The RBFN output is disposed through the following equation where b is a bias:

$$u_n = f(u_p) = b + \sum_{j=1}^{h} \alpha_j \varphi_j(u_p). \tag{27}$$

Here, Gaussian function φ_j of the jth hidden neuron stated in the consecutive mode is

$$\varphi_j(u_p) = \exp\left(-\frac{\|u_p - \mu_j\|^2}{\sigma_j^2}\right) \tag{28}$$

where $\|\cdot\|$ designates the Euclidean norm.

The distribution of the new hidden neurons is the process in the EMRAN algorithm learning. When there are no hidden neurons, $j = 0$ and the RBFN process starts. The RBFN emerges in terms of three major specifications for each of the input and output training data u_p and u_n that are well-informed. The three main equations are

$$e = \|\theta_r - \theta_l\| > \varepsilon_1 \tag{29}$$

$$\|u_{p,i} - \mu_j\| > \varepsilon_2 \tag{30}$$

$$e_{rms,i} = \sqrt{\frac{1}{M}\sum_{n=i-(M-1)}^{i} e^2} > \varepsilon_3 \tag{31}$$

where the desired displacement and actual load displacement output are θ_r and θ_l at each time index i separately in which e refers to the current estimation error standards, where it must be huge enough compared to the threshold and the error threshold illustrated by ε_1, ε_2, and ε_3 that are required to be appointed appropriately by a trial and error method of the user.

The remaining nodes will be determined by whether the nodes are not acceptable to get the network outputs that will assure the error indication ε_1 is stated in (29). The new node summed is far enough from all the current nodes that can be assured when (30) is used. The implementation of (31) is used to verify and resolve whether existing nodes convene the required mean squared error specification or not, and reduce the effect of error in the network growth for the past M outputs. A new hidden neuron can be summed up to the network when all the three equations are contented.

An adaptive rule is implemented via the above three specifications in real time, so that the RBFN parameters w can be modified. Thus, the error between the desired displacement and the real displacement $(\theta_r - \theta_l)$, is minimized throughout the training process. The extended Kalman filter (EKF) will be employed when the equations (29) – (31) are not fulfilled because only the hidden neurons or "winner' neurons are selected. As a result, the value of center μ_j and width σ_j will be enhanced through the EKF. In this paper, a clear approach from [39] has been selected to explain the function of EKF by modifying the weight in EMRAN. Next, the parameter of the network of radial basis function $w^* = f(\mu^*, \sigma^*, b, \alpha^*)$ is improved for the EKF as a referring equation :

$$w_i^* = w_{i-1}^* + \boldsymbol{K}_i^*(\theta_r - \theta_l). \tag{32}$$

From (32), $\boldsymbol{K}_i^*$ shows the Kalman filter gain matrix, as explained in the following:

$$\boldsymbol{K}_i^* = \boldsymbol{P}_{i-1}^* \boldsymbol{B}_i^* [\boldsymbol{R}_i + \boldsymbol{B}_i^{*\mathrm{T}} \boldsymbol{P}_{i-1}^* \boldsymbol{B}_i^*]^{-1} \tag{33}$$

where $\boldsymbol{R}_i$ is the variance noise measurement, whereas $\boldsymbol{P}_i^*$ represents the error of the covariance matrix, and $\boldsymbol{B}_i^*$ expresses the Gaussian function $\boldsymbol{f}(u_{p,i})$ gradient matrix considering the network parameters w^* where w_{i-1}^* can be determined with the following equation:

$$\boldsymbol{B}_i^* = \nabla_{w^*} \boldsymbol{f}(u_{p,i}). \tag{34}$$

Generally, the parameters of RBFN w^* are trained online in terms of the actual parameters of the plant. Nevertheless, in this paper the focus will be on the simulation process. Hence, the parameters given in [1] will be utilized. To train the RBFN, the square-type signal is selected with many types of inputs and practiced. When the training operation is completed, the last weight of the RBFN is kept and will be reused again in order to stimulate the feedback control law u_n. The process is rerun until the process is adequate enough for the three main growth networks.

4. Result and discussion

4.1 Scenario description

The most important part of this study is the application of a high-precision positioning system which is a functional method for researchers and engineers so that a simple and easy controller can be created. The NCTF control concept states that the controller is assembled by a clear and easy open-loop response of an actual system; so it will involve the nonlinearities, i.e. actuator saturation and friction that show the actual behavior of the plant.

The proposed NCTF controller described and expressed is applied for two-mass rotary PTP positioning systems through 30° and 90° step input of simulation that represents the required output. There are two states where the parameters of the mechanism are used throughout the simulation process. The first state is enlarging the inertia of the load and the second state is by the normal load that is the nominal object parameter as illustrated in Table 2 in attention to analyze the potency and robustness of the suggested compensator in the NCTF controller scheme. Both potency and robustness of the positioning are analyzed within the four aspects which are steady state error, percentage of overshoot and settling time. The time is set within 5 s for the system to undergo the simulation process.

Table 2 Object parameter comparison

Load object	Load inertia
Nominal load/kg·m^2	$J_l = 14.17 \times 10^{-6}$
Increased load inertia	$2 \times J_l$
	$5 \times J_l$

4.2 Simulation results

By referring to the simulation results from Fig. 6, the simple open-loop response is shown. On the other hand, NCT gives the inclination and the highest error rate which are 81.169 s^{-1} and 156.8 rad/s respectively with the input actuator to the system which operates at 12 V. Because of mechanical resonance, the load object responses will vibrate. The vibrating frequency ω_{fd} is given as 40 Hz. In this paper the Roth-Hurwitz stability criterion is used to calculate the NF parameters so that a stable and continuous closed-loop system can be obtained, as a result of constraint to be satisfied [21]:

$$2\zeta_o\omega_o \geqslant -\alpha. \tag{35}$$

Thus, 0.7 Hz and 40 Hz of the numerical factors for the numerator of NF (ζ_f and ω_f) are chosen while 0.9 Hz and 60 Hz of the denominators (ζ_o and ω_o) of NF are chosen respectively. From (20) and (21), the gain parameters for the PI compensator produce $K_p = 4.79 \times 10^{-1}$ and $K_i = 2.65 \times 10^{-1}$ separately with the design parameters for ζ and ω_n selected as 9.5 and 10.5 respectively. As for the FL compensator based on (26), the fuzzy gain produces $K_{fz} = 3.25$.

A different load object that starts from the nominal inertia J_l has been operated on the plant. Later, we increase it by two times $(2 \times J_l)$ and five times $(5 \times J_l)$ with continous friction at the highest friction factor T_{fmax}. A comparison of the controllers is presented in the Figs. 17 – 20 in which the controllers are evaluated in terms of positioning as well as the robustness of performances where the step input to the system is set for 30° and 90°. The motioning performances for both nominal and enlarged load object inertia rely on settling time, percentage of overshoot and positioning accuracy that are illustrated in Table 3.

From the results tabulated in Table 3, for the step input of the nominal load object of 30° and 90°, the NCTF-EMRAN generates the minimum percentage of overshoot than NCTF-PI and NCTF-FL. Meanwhile NCTF-FL gives the fastest settling time among the three controllers. Every controller requires zero error in which NCTF-PI gives the small error of 0.08° for 30° step input in terms of steady-state analysis. The nominal object inertia is increased by five times as shown in Fig. 19 and Fig. 20. From the results we can see that the NCTF-EMRAN controller allows the smallest percentage of overshoot and is tailed by the remaining controllers which are NCTF-FL and NCTF-PI.

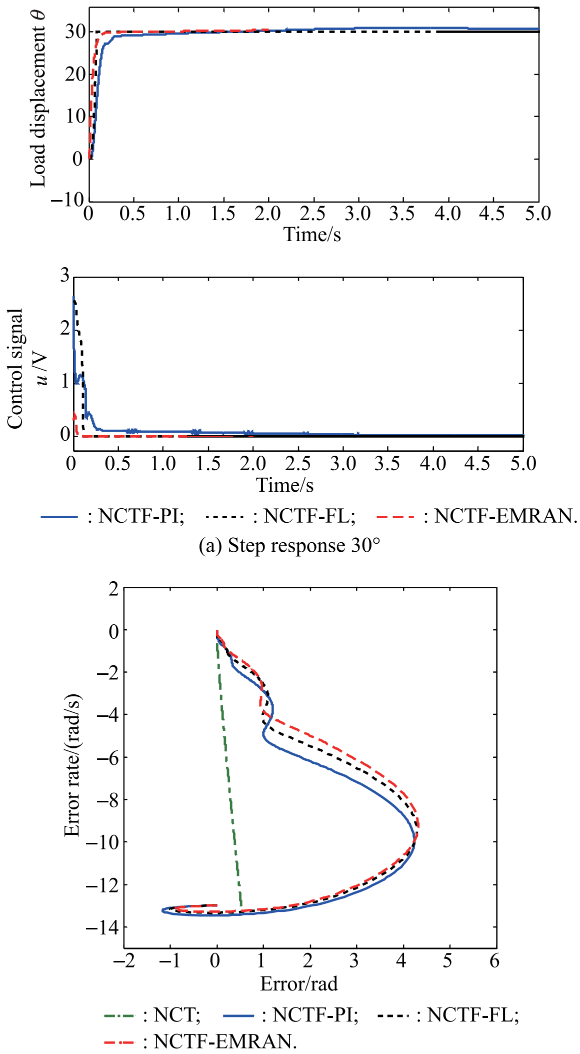

(a) Step response 30°

(b) Object motion for 30° step input

Fig. 17 Step response comparison of nominal object (30°)

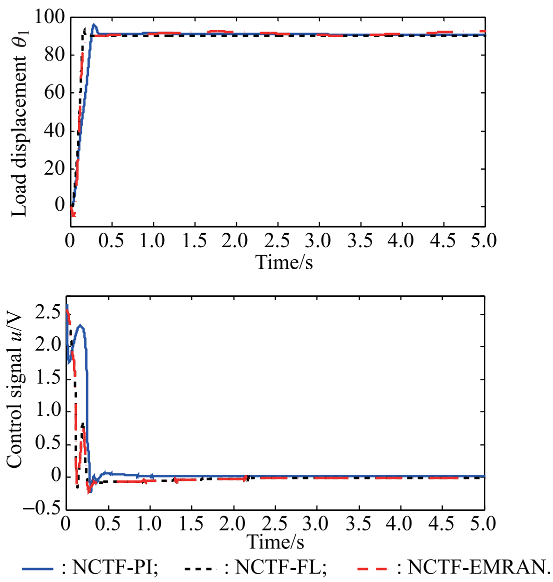

(a) Step response 90°

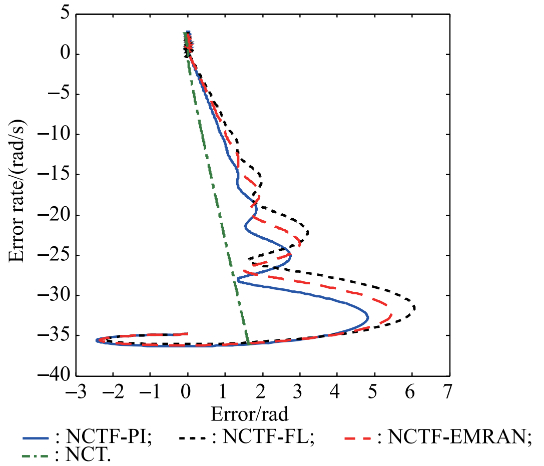

(b) Object motion for 90° step input

Fig. 18 Step response comparison of nominal object (90°)

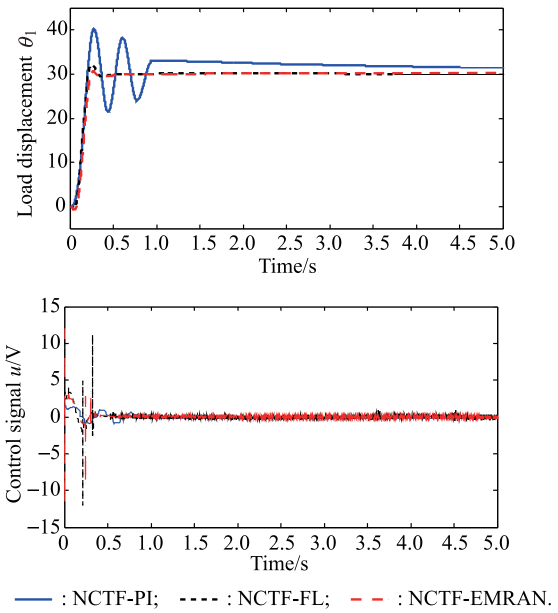

(a) Step response 30°

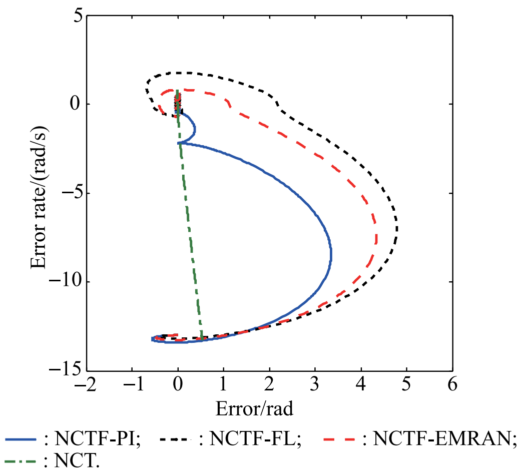

(b) Object motion for 30° step input

Fig. 19 Step response comparison of increased inertia object ($5 \times J_l$) (30°)

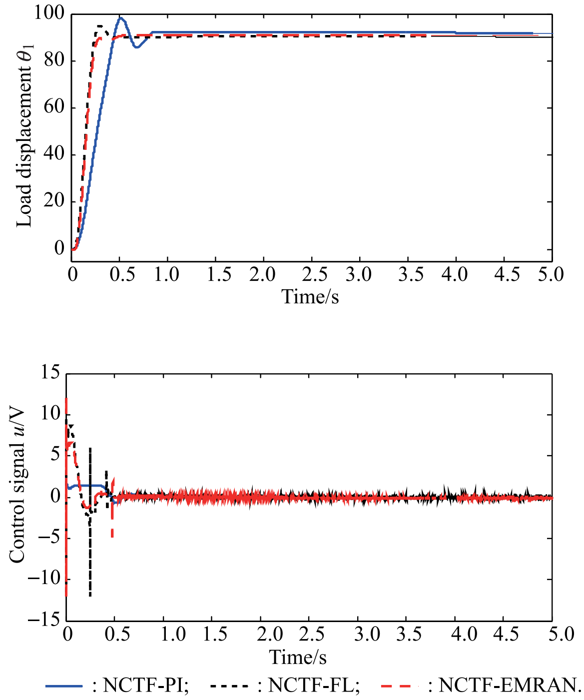

(a) Step response 90°

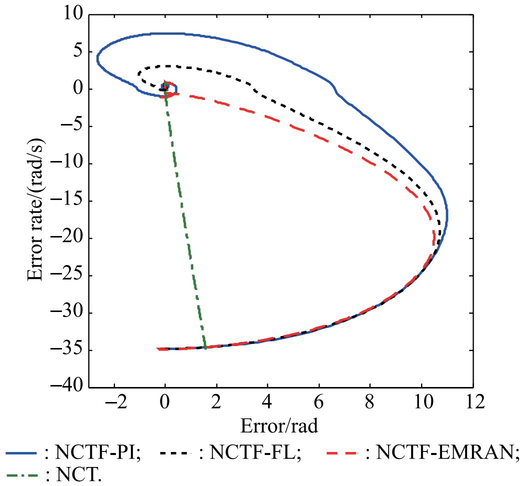

(b) Object motion for 90° step input

Fig. 20 Step response comparison of increased inertia object ($5 \times J_l$) (90°)

Besides, during the time that object inertia is increased by two to five times, the NCTF-FL takes the shortest time to settle down the vibration compared to NCTF-PI and NCTF-EMRAN. This scenario can be seen clearly in Table 3. Furthermore, NCTF-PI has a severe response compared to NCTF-FL and NCTF-EMRAN in case of the positioning accuracy for increased inertia. Still, although the control signal is saturated, the response is stable for all types of NCTF controllers and in contrast, when PID controllers are used, the results are in unstable responses as shown and described in [21] for increased object inertia.

Table 3 Positioning performance comparison of increased load inertia

Load inertia	Input/(°)	Compensator	Overshoot/%	Settling time/s	Steady-state error/(°)
J_l	30	PI	0.01	0.761	0.08
		FL	0	0.230	0
		EMRAN	0	0.270	0
	90	PI	6.4	0.335	0
		FL	0.5	0.201	0
		EMRAN	0.05	0.210	0.01
$2\times J_l$	30	PI	6.9	0.910	0.07
		FL	1.2	0.420	0.06
		EMRAN	0.5	0.440	0.04
	90	PI	7.2	0.440	0.45
		FL	2.0	0.350	0.10
		EMRAN	1.24	0.401	0.05
$5\times J_l$	30	PI	33.9	1.290	0.14
		FL	10	0.50	0.08
		EMRAN	6	0.450	0.10
	90	PI	8.5	0.765	0.52
		FL	6.0	0.505	0.1
		EMRAN	1.3	0.505	0.14

Moreover, the NCTF control concept in Section 2 that is explained in the discussion can be shown in Figs. 17 – 20. The object motion is required to follow the trajectory shown by the NCT and terminated at the origin for all types of the NCTF controller. The proposed controllers which are NCTF controllers are robust to inertia variation since it is already proven by the results with different input targets. Even though most of the positioning performances are much better when using the NCTF-EMRAN controller, it also has a few weaknesses in the design part of the controller. Some disadvantages found in the design and iteration process cost more time in the simulation so that it can control the systems. Therefore, it can be seen as non-practical in real application implementations. Therefore the EMRAN iteration process is not highlighted in this paper.

4.3 Experimental results

The stepwise input is applied to the object. The input to the actuator u_r is 12 V. The experiments are handled in two conditions only: with normal load and with increased load inertia as displayed in Fig. 21 and illustrated in Table 2. Normal object is defined as the two-mass experimental rotary positioning with the nominal object parameter.

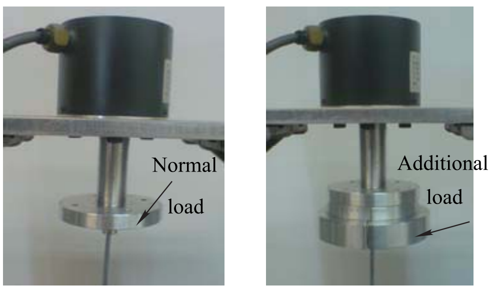

Fig. 21 Nominal and increased object inertia

As simulated, first, we operate the system starting with nominal inertia; then, we increase it by five times and ten times with constant maximum friction. We analyze and estimate the controllers based on positioning and robustness performances for 30° and 90° step input to the system as shown in Figs. 22 – 25. Table 4 demonstrates the controllers' positioning performances for nominal and increased load object inertia in terms of percentage overshoot, settling time, and positioning accuracy. An average of 20 similar experiments is conducted.

For nominal load object as shown in Fig. 22 and Fig. 23 for 30° and 90° step input, and from Table 4, the NCTF-FL and NCTF-PI controllers give the smaller percentage of overshoot compared to NCTF-EMRAN. However, NCTF-EMRAN has the fastest settling time between the two controllers. As for the steady-state analysis, all the three controllers denote some error with NCTF-PI showing a smallest error of 0.02° for 30° step input. Next, when the object is conducted for 90° step input, NCTF-EMRAN shows the smallest overshoot with the smallest steady-state error, while NCTF-FL shows unstable performance due to the design of the fuzzy rules. The results shown in Fig. 24 and Fig. 25 express the increment of the nominal object inertia for ten times, and NCTF-EMRAN produces the minor percentage of overshoot and followed by the NCTF-FL, whereas NCTF-PI gives the unstable output performances.

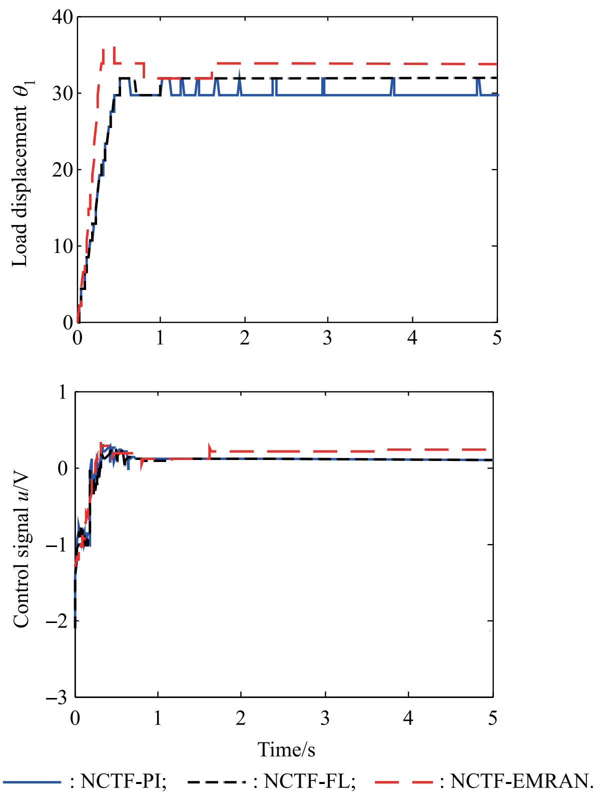

Fig. 22 Step response 30° comparisons of nominal object

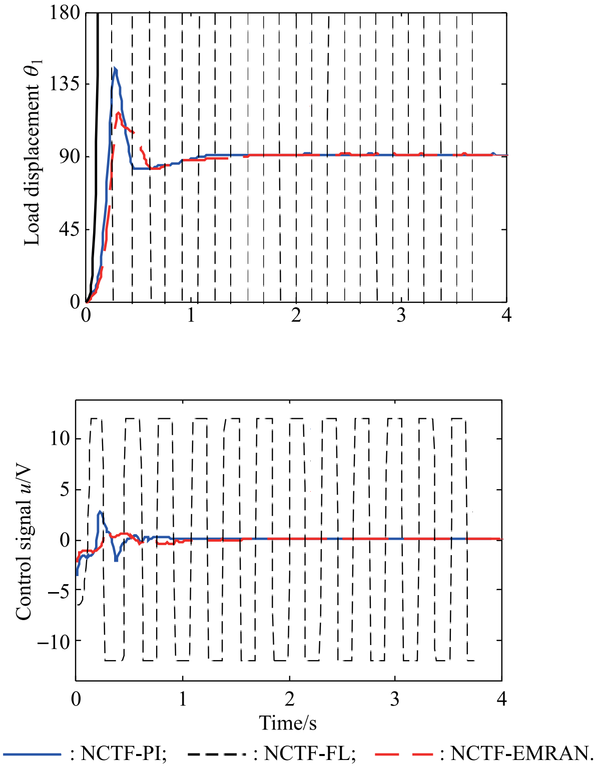

Fig. 23 **Step response 90° comparison of nominal object**

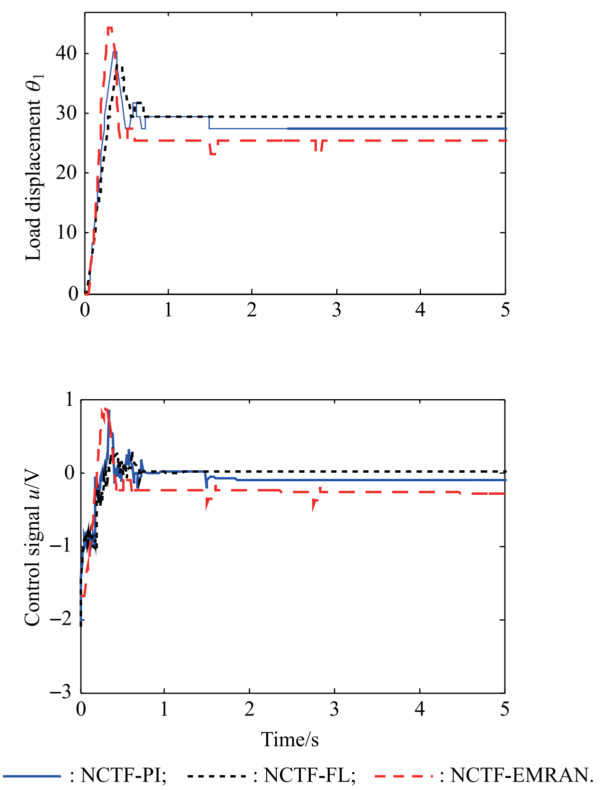

Fig. 24 **Step response at 30° comparison of increased inertia object ($10 \times J_l$)**

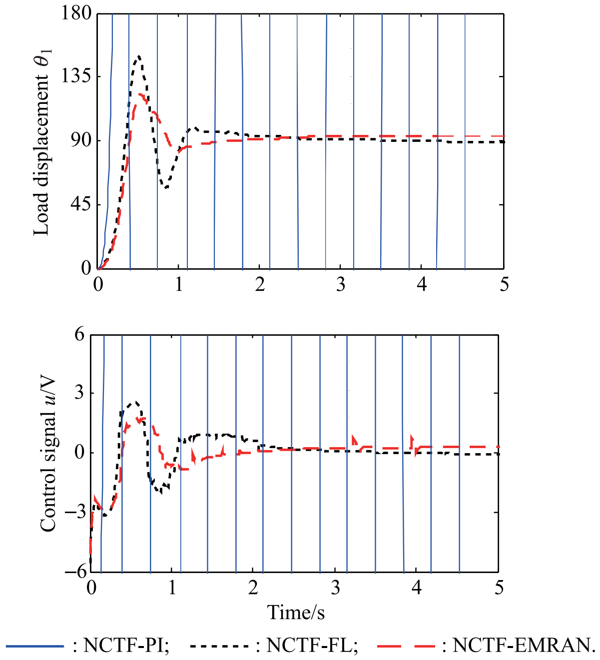

Fig. 25 **Step response at 90° comparison of increased inertia object ($10 \times J_l$)**

Table 4 **Experimental positioning averaged performance comparison**

Load inertia	Input/(°)	Compensator	Overshoot/%	Settling time/s	Steady-state error/(°)
J_l	30	PI	0.01	0.74	0.02
		FL	0.01	0.26	0.04
		EMRAN	0.1	0.24	0.10
	90	PI		Unstable	
		FL	44.8	0.201	0.02
		EMRAN	24.8	0.210	0.01
$5 \times J_l$	30	PI	6.9	0.82	0.02
		FL	7.2	0.44	0.10
		EMRAN	10.5	0.42	0.12
	90	PI		Unstable	
		FL	50.4	0.350	0.04
		EMRAN	24.6	0.401	0.02
$10 \times J_l$	30	PI	28.8	1.04	0.04
		FL	30.2	0.85	0.14
		EMRAN	45.6	0.64	0.16
	90	PI		Unstable	
		FL	56.8	0.505	0.04
		EMRAN	26.4	0.505	0.02

In addition, from Table 4, it can be seen that when the object inertia is increased by five and ten times, NCTF-EMRAN produces the rapid settling time compared to the other two controllers. However, NCTF-EMRAN demonstrates poor steady state error when object is driven in 30° step input which results in different (best) performances in 90° step input. Moreover, in terms of the positioning accuracy for increased inertia, NCTF-PI has a worse response compared to NCTF-FL and NCTF-EMRAN particularly in 90° step input. However, in large input position, NCTF-PI yields unstable response either for nominal or increased object load. For intelligent based controllers, the response is stable, even if the control signal is saturated.

Unlike the intelligent based method, for the two-mass rotary system, the NCTF-PI controller results in a vibrating response with a frequency of 40 Hz particularly in 90° step input. This vibration is caused by mechanical resonance of the system. Thus, the proposed NCTF controller effectively attenuates this vibration problem and is much more robust to inertia variations compared with the NCTF-PI controller. The NCTF controller shows a stable response as well as good performance in positioning accuracy when the object inertia is increased. Moreover, the controller results in a positioning accuracy close to the sensor resolution which is 0.036 rad when it is carried out by experiment.

5. Conclusions

This paper designates a practical control approach for motion system application using the two-mass rotary positioning systems. First, the NCT is determined from the load responses. The vibrating responses are averaged applying a simple MAV filter in order to exclude the influence of the vibration on the NCT. Then, the proposed compensators, i.e. PI, FL, and EMRAN, with NF, are constructed and established through the NCT parameters and the object responses information with the aim of forcing the object motion to reach the NCT as fast as possible, and to control the object motion in order to follow the NCT as closely as possible and stop at the origin. The NF is selected in order to cancel the vibration frequency created by the mechanical resonance of the system.

Throughout the simulations and the experiment that has been carried out, the results of the propose controllers are evaluated and compared in terms of their positioning with load variations. The robustness of the controllers is also well evaluated and explained. The simulation confirms that NCTF-EMRAN and NCTF-FL show improved motion performance in terms of percentage of overshoot, settling time, and positioning accuracy than the conventional NCTF-PI controller. However, NCTF-PI is easier and simpler in terms of controller design than the other two controllers.

Finally, an appropriate control method for fuzzy rules design needs to be considered. An adaptive neuro-fuzzy inference system controller needs to be considered as an alternative controller instead of using an EMRAN as a control approach.

Acknowledgment

The first author would like to thank the late Prof. Wahyudi Martono and Prof. Rini Akmeliawati for imparting such good knowledge related to this research as his master student.

References

[1] P. H. Jui. Load effect on the vibration characteristics of a stage with rolling guides. *Journal of Mechanical Science and Technology*, 2009, 23(1): 89 – 99.

[2] F. Al-Bender, W. Symens, J. Swevers, et al. Theoretical analysis of the dynamic behaviour of hysteresis elements in mechanical systems. *International Journal of Non-Linear Mechanics*, 2004, 39(1): 1721 – 1735.

[3] M. Shoeybi, M. Ghorashi. Nonlinear vibration control of a system with dry friction and viscous damping using the saturation phenomenon. *Nonlinear Dynamics*, 2006, 45(3/4): 249 – 272.

[4] K. Sato, G. J. Maeda. Fast precision positioning of a ball screw mechanism on practical NCTF control. *International Journal of Automation Technology*, 2009, 3(3): 233 – 240.

[5] M. Jouaneh, P. Ge. Modeling and control of micro-positioning tower. *Mechatronics*, 1997, 7(5): 465 – 478.

[6] S. B. Chang, S. H. Wu, Y. C. Hu. Submicrometer overshoot control of rapid and precise positioning. *Precision Engineering*, 1997, 20(3): 161 – 170.

[7] P. J. Serkies, G. Tarchla. Predictive position control in two-mass drive with induction motor over a wide range of speed changes. *Computer Applications in Electrical Engineering*, 2012, 10(1): 146 – 157.

[8] S. Wu, J. Fu. Time-optimal control of servo system using PD algorithms. *JSME International Journal*, 1998, 41(3): 384-390.

[9] Y. F. Li, J. Wikander. Model reference discrete-time sliding mode control of linear servo motor precision servo systems. *Mechatronics*, 2004, 14(7): 835 – 851.

[10] K. K. Tan, H. L. Lee, H. F. Dou, et al. Precision motion control with disturbance observer for pulse width modulated driven permanent magnet synchronous motors. *IEEE Trans. on Industrial Electronics*, 2005, 52(3): 814 – 823.

[11] N. Nath, B. Roy, A. Choudhury. Transient performance characteristics of control systems. *International Journal of Control*, 1972, 16(3): 509 – 512.

[12] M. Maki, K. Hagino. Robust control with adaptation mechanism for improving transient behaviour. *International Journal of Control*, 1999, 72(13): 1218 – 1226.

[13] Z. Lin, R. Mantri, A. Saberi. Semi-global output regulation for linear systems subject to input saturation a low and high gain design. *Proc. of American Control Conference*, 1995: 3214 – 3218.

[14] W. A. Malik, S. Darbha, S. P. Bhattacharyya. On controlling the transient response of linear tim invariant systems with fixed structure controllers. *Asian Journal of Control*, 2012, 14(6): 1643 – 1648.

[15] Z. Lin, M. Pachter, S. Banda. Toward improvement of tracking performance nonlinear feedback for linear systems. *International Journal of Control*, 1998, 70(1): 1 – 11.

[16] G. Cheng, K. Peng. Robust composite nonlinear feedback control with application to a servo positioning system. *IEEE Trans. on Industrial Electronics*, 2007, 54(2): 1132 – 1140.

[17] W. Y. Lan, Q. Zhou. Speed control of DC motor using composite nonlinear feedback. *Proc. of IEEE International Conference on Control and Automation*, 2009: 2160 – 2164.

[18] M. Wahyudi, K. Sato, A. Shimokohbe. New practical control method for PTP positioning systems: robustness evaluation. *Proc. of the 10th International Conference on Precision Engineering*, 2001: 774 – 778.

[19] M. Wahyudi, K. Sato, A. Shimokohbe. Robustness evaluation

of new practical control method for PTP positioning systems. *Proc. of the IEEE/SME International Conference on Advanced Intelligent Mechatronics*, 2001: 843 – 848.

[20] M. Martono. New practical control of PTP positioning systems. Tokyo, Japan: Tokyo Institute of Technology, 2002.

[21] K. Sato. Practical control of precision positioning mechanism with friction. *Precision Engineering*, 2004, 28(4): 426 – 434.

[22] J. M. Guilherme, K. Sato. Practical control method for ultra-precision positioning using a ballscrew mechanism. *Journal of Precision Engineering*, 2008, 32(4): 309 – 318.

[23] K. Sato, G. J. Maeda. A practical control method for precision motion – improvement of NCTF control method for continuous motion control. *Journal of Precision Engineering*, 2009, 33(3): 175 – 186.

[24] S. H. Chong, H. Hashimoto, K. Sato. Practical motion control with acceleration reference for precision motion — new NCTF control and its application to non-contact mechanism. *Precision Engineering*, 2001, 35(1): 12 – 23.

[25] W. S. Kim, D. J. Lee, S. K. Lee. Influence of a high vacuum on the precise positioning using an ultrasonic linear motor. *Review of Scientific Instruments*, 2011, 82(1): 1 – 10.

[26] K. Sato, Y. Sano. Practical and intuitive controller design method for precision positioning of a pneumatic cylinder actuator stage. *Precision Engineering*, 2014, 38(4): 703 – 710.

[27] M. F. M. Yakub. Development of practical control method for two-mass positioning systems. Kuala Lumpur, Malaysia: International Islamic University Malaysia, 2011.

[28] W. Martono, K. Sato, A. Shimokohbe. Characteristics of practical control for point to point (PTP) positioning systems effect of design parameters and actuator saturation on positioning performances. *Precision Engineering*, 2003, 27(2): 157 – 169.

[29] W. Martono, K. Sato, A. Shimokohbe. Robustness evaluation of three friction compensation methods for point-to-point (PTP) positioning systems. *Robotics and Autonomous Systems*, 2005, 52(2): 247 – 256.

[30] S. H. Chong, K. Sato. Practical controller design for precision positioning, independent of friction characteristic. *Journal Precision Engineering*, 2009, 34(2): 286 – 300.

[31] L. Sato. Practical and intuitive controller design for precision motion – AR-CM NCTF control of ball screw mechanism. *International Journal of Automation Technology*, 2011, 5(6): 793 – 799.

[32] F. Yakub, R. Akmeliawati. Study review on nominal characteristic trajectory following controller for point-to-point positioning systems. *Proc. of the 7th International Conference on Industrial Electronics and Applications*, 2011: 1945 – 1950.

[33] S. H. Chong, K. Sato. AR-CM NCTF control for precision positioning systems — concept and results. *Proc. of the 6th Asia Modelling Symposium*, 2012: 156 – 160.

[34] F. Yakub, R. Akmeliawati, A. Abu. Practical control method for two-mass rotary point-to-point positioning systems. M. Vagia. *PID controller design approaches – theory, tuning and application to frontier areas*. Croatia: InTech, 2012: 159 – 184.

[35] M. Wahyudi, T. F. Ibrahim, R. Muhida, et al. Robust fuzzy-based NCTF controller of point-to-point positioning systems. *International Journal of System Simulation*, 2007, 1(1): 11 – 29.

[36] M. Wahyudi, A. Albagul. Performance improvement of practical control method for positioning systems in the presence of actuator saturation. *Proc. of the IEEE International Conference on Control Applications*, 2004: 296 – 302.

[37] H. Azami, K. Mohammadi, B. Bozorgtabar. An improved signal segmentation using moving average and savitzky-golay filter. *Journal of Signal & Information Processing*, 2012, 3(1): 39 – 44.

[38] C. Plett, M. A. Copeland. Self-tuned continuous-time notch filters. *Journal of VLSI Signal Processing*, 1994, 8(3): 227 – 240.

[39] M. Birgmeier. A fully kalman-trained radial basis function network for nonlinear speech modelling. *Proc. of IEEE International Conference on Neural Networks*, 1995: 259 – 264.

Biographies

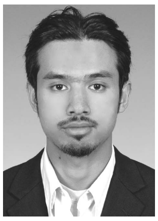

Fitri Yakub received his Dip.Eng and BEng degrees in mechatronics engineering and electronics engineering from University of Technology Malaysia in 2001 and 2006 respectively. He obtained his M.S. and Ph.D. degrees in mechatronics engineering from International Islamic University Malaysia and Tokyo Metropolitan University in 2011 and 2015 respectively. He is now with Malaysia-Japan International Institute of Technology. He is a senior member of IEEE and member of IET, SAE, and SICE. He was recipient of an Asian Human Resource Fund by Tokyo Metropolitan Government from 2012 to 2015.
E-mail: mfitri.kl@utm.my

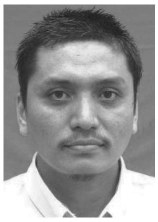

Shamsul Sarip received his Dip.Eng, BEng, and MEng degrees in mechanical engineering from University of Technology Malaysia (UTM) in 1995, 1998, and 2002 respectively. He obtained his Ph.D. degree in mechanical engineering from Bradford University in 2011. He is now with Razak School of Engineering and Advanced Technology, UTM. His research interests include lightweight friction brakes, braking performance, regenerative braking, heat transfer, finite elements method, vehicle dynamics, and vehicle design.
E-mail: shamsuls.kl@utm.my

Andika Aji Wijaya received his B.S. degree in mechanical engineering from Bandung Institute of Technology Indonesia in 2006. He obtained his M.S. degree in mechatronics engineering from International Islamic University Malaysia in 2009. Since 2010, he has been with University of Business & Technology Saudi Arabia as a lecturer. His field of research interest includes active vibration control, motion control, control system, and intelligent system.
E-mail: andika@ubt.edu.sa

Yasuchika Mori received his B.S., M.S. and Ph.D. degrees in electrical engineering from Waseda University in 1976, 1978, and 1981 respectively. From 1981 to 1987, he worked as a researcher in the R&D Center of Toshiba Corporation. From 1988 to 1992, he worked as an associate professor at Saitama University, Japan and National Defense University, Japan from 1993, and as a full professor in 1999. He is a professor at Tokyo Metropolitan Institute of Technology in 2003 and since 2005, he has been with the Department of Human Mechatronics System at the Graduate School of System Design, Tokyo Metropolitan University. He is a member of IEEE, ISCIE, senior member of IEEJ, and Fellow of SICE. His field of research interest includes digital control and design, automatic and robust control, stochastic control, and RFID.
E-mail: ymori@tmu.ac.jp